Eur. Phys. J. D **24**, 261–263 (2003)
DOI: 10.1140/epjd/e2003-00107-8

THE EUROPEAN PHYSICAL JOURNAL D

Plasma desorption mass spectroscopy of thiol-passivated gold nanoparticles

Y. Tai[1,a], J. Murakami[1], K. Saito[1], M. Ikeyama[1], K. Tajiri[1], M. Watanabe[1,2], S. Tanemura[2], and T. Mizota[3]

[1] Chubu Research Base, National Institute of Advanced Industrial Science and Technology, Nagoya 463-8560, Japan
[2] Nagoya Institute of Technology, Nagoya 466-8555, Japan
[3] Tsukuba Nanotechnology Co Ltd., Tsukuba 305-0035, Japan

Received 10 September 2003
Published online 3 July 2003 –

Abstract. Plasma desorption mass spectrometry has been applied to characterization of dodecanthiol-passivated gold nanoparticles. An overview of the experimental set-up and mass analyses for the nanoparticles prepared in different conditions are shown. Mass distributions were found to shift to higher mass regions with increasing reaction temperature and reaction period. The results are consistent with those of transmission electron microscopy observations, UV-visible absorption spectra and also with a reported laser desorption mass spectrometry.

PACS. 36.40.-c Atomic and molecular clusters – 39.90.+d Other instrumentation and techniques for atomic and molecular physics – 61.46.+w Nanoscale materials: clusters, nanoparticles, nanotubes, and nanocrystals

1 Introduction

Small metallic particles are chemically active, and because of this property, some of them are used as catalysts for various chemical reactions. The smaller analogues, metal clusters (or nanoparticles), are also reactive with gaseous molecules and, in some cases, the reactivity differs by orders of magnitude depending on cluster size [1–4]. Thus, if an ensemble of clusters with a specific size is available, it would work as a very efficient catalyst. Motivated by this, we have been trying to prepare monodispersed metal nanoparticles with less than 2 nm diameter and disperse them in highly porous matrices [5].

For developing the size-selective synthesis of nanoparticles, reliable methods for evaluating particle size distributions are strongly desired. Conventionally, averaged particle diameters have been evaluated using the width of X-ray or electron diffraction peaks, plasmon band width in UV-vis absorption spectra, and transmission electron microscopy (TEM) images. In recent years, mass spectrometry has been introduced to diagnose size distributions of chemically prepared nanoparticles. Whetten *et al.* have utilized laser desorption time-of-flight (LD-TOF) measurements for mass analyses of thiol-passivated gold nanoparticles and demonstrated that mass spectroscopy gives information on particle size which is difficult to know from TEM or optical absorption measurements [6,7].

Recently, we have constructed a plasma desorption (PD)-TOF mass spectroscopic system. Highly charged ions from a 1.7 MV tandem ion accelerator, routinely Si^{6+} (11.9 MeV), are used for ionization and desorption of samples [8]. PDMS is a powerful tool for diagnosing structures of large organic molecules since target molecules are rather undamaged in the PD process initiated by electronic stopping of primary ions. Nowadays, ^{252}Cf PDMS is used as a complementary method for matrix assisted laser desorption ionization (MALDI) mass spectrometry for characterization of biological substances. The characteristics of our instrument is to use an ion accelerator for generation of primary ions; thus, by changing element, charged state, and acceleration voltage, we can select the PDMS or SIMS mode.

In this report, we will describe the experimental set-up, and mass spectra obtained for dodecanethiol passivated gold nanoparticles ($Au_x(DDT)_y$) prepared in various conditions. The mass spectra were found to be consistent with the particle size distributions obtained from TEM observations and optical absorption measurements.

2 Experimental

2.1 The PD-TOF system

Details of the PD-TOF system will be reported elsewhere and thus, is described here briefly [8]. Figure 1 shows a block diagram of the experimental set-up. The instrument consists of two primary beam detectors (PBD1 and 2) which generate a start pulse for the TOF measurement, a TOF tube, and a signal processing unit. $^{28}Si^{6+}$ (11.9 MeV)

[a] e-mail: tai.y@aist.go.jp

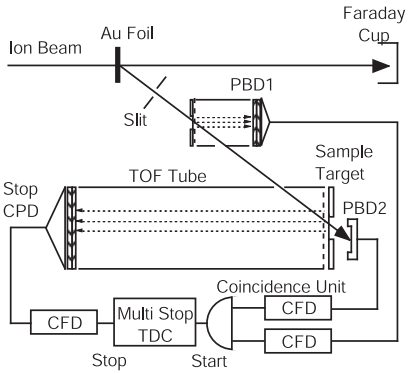

Fig. 1. Block diagram of the PDMS equipment.

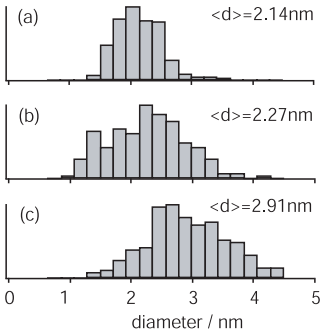

Fig. 2. Core size distributions obtained from TEM images for samples prepared at (T_r, D_r) = (273 K, 1 min) (a), (273 K, 180 min) (b), (313 K, 180 min).

from a tandem ion accelerator is elastically scattered from a gold foil target. Scattered ions with a scattering angle of 45° go through a slit and are fed to the TOF system. The ions pass through a Au coated polyvinyl formal (FORMVAR) film, which emits electrons, in front of PBD1. The electrons are accelerated to 2 keV and detected by a dual microchannel plate detector. The primary ions then collide with a target material dispersed on a Au coated myler film (thickness: 1.8 μm), typically floated to + or −10 kV. The secondary ions are accelerated by a single field and drift in a 20 cm long TOF tube and hit a dual microchannel detector (Stop CPD). At the backside of the sample target, PBD2, a solid state ion detector is placed.

Signals from PBD1 and 2 are transformed to TTL pulses and a coincidence signal is generated. The signal is used as a trigger signal for a multi-stop time to digital converter (TDC) installed in a PC. Stop CPD signals are accumulated on the multi-stop TDC. Mass resolution of ≈1000 was obtained at $m/e = 720$ (C_{60}).

The secondary ion yield of the gold nanoparticles was 0.2–0.5 per primary ion. For evaluating the yield, ion counts integrated for a mass range corresponding to the nanoparticles were divided by the number of start signals. Thus, the yield includes all the parameters such as ion transmission and detection efficiencies specific to the equipment. Secondary ion signals were accumulated for $2-6 \times 10^6$ incidences of primary ions for obtaining mass spectra.

2.2 Preparation of thiol-passivated gold nanoparticle

$Au_x(DDT)_y$ was prepared according to the method of Brust *et al.* [9]. Briefly, $AuCl_4^-$ ion was extracted to a toluene phase by excess tetraoctylammonium bromide and reduced with sodium borohydride in the presence of dodecanethiol. The molar ratio of Au atom and dodencanethiol was 1:3. The reaction was performed at temperatures (T_r) of 273 and 313 K with reaction times (D_r) of 1 and 180 min. The product was washed with ethanol and purified two times by recrystallization from a toluene/ethanol mixed solvent (1:40 in volume) at 255 K. The product was waxy solid with black-purple color. For the PD-TOF measurements, the toluene solution of the particles were dropped on the gold coated myler film and dried. The thickness of resultant nanoparticle films was 3–6 μm.

2.3 Other characterization methods

TEM images were taken by Hitachi H8000 with a LaB_6 filament operated at 200 kV. $Au_x(DDT)_y$ toluene solution was dried on a carbon film for the observation.

UV-vis spectra were recorded on the Parkin-Elmer Lambda18 spectrometer.

3 Results and discussion

Figures 2a–2c show histograms of the particles size distributions obtained from TEM images for $Au_x(DDT)_y$ nanoparticles prepared under three different reaction conditions: (T_r, D_r) = (273 K, 1 min) (a), (273 K, 180 min) (b), (313 K, 180 min) (c). About 200 particles were sampled from the TEM images. The obtained average diameters for Figures 2a, 2b and 2c were 2.14, 2.27, and 2.91 nm, respectively. It has been reported that higher reaction temperature and longer reaction time promote the particle growth [7]. This probably explain the trend of increasing average size of the particles from Figures 2a–2c. However, when Figures 2a and 2b is compared, the number of smaller particles seem to be enhanced in Figure 2b. Since a limited number of particles were sampled for making the histograms, it is not clear if such a difference really exists. To clarify this point, optical absorption and PD-TOF measurement was performed.

Figure 3 shows UV-vis optical absorption spectra for the samples of Figures 2a–2c in toluene. The spectra showed a broad absorption (plasmon band) around 510 nm superimposed on that of transitions from 5*d* to 6*sp* bands [7]. It is known that the intensity of plasmon band increases with the metal particle size [10,11]. As shown in the figure, plasmon band is most clearly visible in spectrum (c) which is for the sample prepared at 313 K. This is consistent with the size distribution from TEM images (Fig. 2) and mass spectra which is shown below in Figure 4. The UV-vis spectra (a) and (b) were almost identical, thus, do not give information on differences in the particle size distributions.

PD-TOF spectra for the samples (a–c) are shown in Figure 4. It is clearly seen that spectrum (c) has a peak in

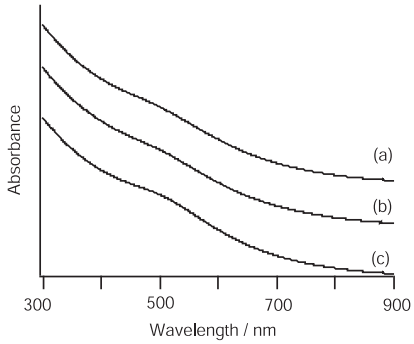

Fig. 3. UV-vis absorption spectra for samples prepared at $(T_r, D_r) = (273\ \mathrm{K}, 1\ \mathrm{min})$ (a), (273 K, 180 min) (b), (313 K, 180 min) (c). The spectra are vertically arranged for clarity.

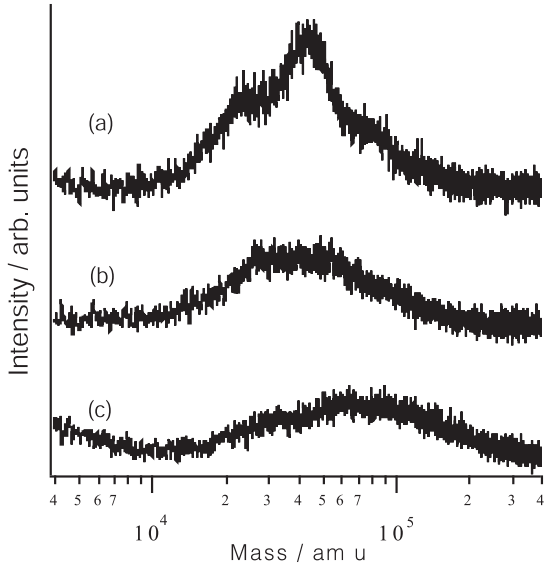

Fig. 4. PD mass spectra for samples prepared at $(T_r, D_r) = (273\ \mathrm{K}, 1\ \mathrm{min})$ (a), $(273\ \mathrm{K}, 180\ \mathrm{min})$ (b), $(313\ \mathrm{K}, 180\ \mathrm{min})$ (c). The spectra are vertically arranged for clarity.

higher mass regions than the other two spectra, which is consistent with the TEM observations and the UV-vis spectra. Spectrum (a) shows peaks or shoulders at $m/e \approx 23k$ ($k = 1000$), $43k$ and $76k$. The shoulder at $\approx 23k$ coincides with a mass peak found in the LD-TOF spectra for $\mathrm{Au}_x(\mathrm{DDT})_y$ particles without separation treatments reported by Schaaff *et al.* [7]. The main peak at $\approx 43k$ corresponds to the core diameter of ≈ 1.8 nm if it is assumed that the gold core is a sphere with the bulk density and a thiol molecule occupies 22 $\mathrm{Å}^2$ on the particle surface as on the bulk Au surface [12]. The mass distribution of spectrum (b) slightly shifted to higher mass region compared with spectrum (a). In spectrum (b), the shoulders at $\approx 23k$ and $\approx 43k$ are not seen, and instead, flat-topped maxima extending from $28k$ to $55k$ are observed. The value $28k$ corresponds to the mass of a compound reported to be obtained in high yield [7].

When size distributions of the passivated gold nanoparticles obtained from TEM images are compared with the PD mass spectra, we often find that the TEM size distributions are broader and the mean diameters are larger than those deduced from mass spectra [8]. For example, the maximum of the mass spectrum (c) is $\approx 72k$ and this value corresponds to ≈ 2.1 nm in diameter. This diameter is smaller than that at the maximum (≈ 2.5 nm) in Figure 2c. There exist several factors that possibly cause the discrepancy. In the TEM observations, aggregation and fusion of particles exposed to electron beams can occur, which can be the cause of larger diameters. On the other hand, in the PD mass spectrometry, fragmentation of nanoparticles by the impact of primary ions and/or the size-dependent detection efficiency of the microchannel plate detector may alter mass distributions. At present, it is not clear which of the above mentioned factors is most important to cause the discrepancy.

Despite the discrepancy, the trends of the PD mass spectra for samples (a–c) coincided with those of the TEM particle size distributions and the optical absorption spectra. Moreover, PD mass spectra most clearly showed the changes in size distributions caused by preparation conditions. These results seem to indicate that PD mass spectrometry works as an efficient tool for the analysis of the passivated metal nanoparticles.

The authors are grateful to Prof. T. Tanji of Nagoya University for TEM observations. Dr. F. Ohashi is acknowledged for optical measurements. This work was partly supported by the core research for evolutional science and technology (CREST) conducted by Japan Science and Technology Corporation (JST).

References

1. S.C. Richtsmeier, E.K. Parks, K. Liu, L.G. Pobo, S.J. Reily, J. Chem. Phys. **82**, 3659 (1985)
2. M. Haruta, N. Yamada, T. Kobayashi, S. Iijima, J. Catal. **115**, 301 (1989)
3. J.M. Alford, R.T. Laaksonen, R.E. Smalley, J. Chem. Phys. **91**, 2618 (1991)
4. A.B. Vakhtin, K. Sugawara, J. Chem. Phys. **115**, 3629 (2001)
5. Y. Tai, M. Watanabe, K. Kaneko, S. Tanemura, T. Miki, J. Murakami, K. Tajiri, Adv. Mater. **13**, 1611 (2001)
6. R.L. Whetten, J.T. Khoury, M.M. Alvarez, S. Murthy, I. Vezmar, Z.L. Wang, P.W. Stephens, C.L. Cleavland, W.D. Luedtke, U. Landman, Adv. Mater. **8**, 428 (1996)
7. T.G. Schaaff, M.N. Shafigullin, J.T. Khoury, I. Vezmar, R.L. Whetten, W.G. Cullen, P.N. First, C. Gutiĕrrez-Wing, J. Ascensio, M.J. Jose-Yacamăn, J. Phys. Chem. B **101**, 7885 (1997)
8. T. Mizota, T. Miki, K. Saito, Y. Tai, M. Ikeyama, K. Tajiri, J. Mirakami, to be published
9. M. Brust, M. Walker, D. Bethell, D.J. Schiffrin, R. Whyman, J. Chem. Soc. Chem. Commun. 801 (1994)
10. K.V. Sarathy, G. Raina, R.T. Yadev, G.U. Kulkarni, C.N.R. Rao, J. Phys. Chem. B **101**, 9876 (1997)
11. G.W. Anold, J. Appl. Phys. **46**, 4466 (1975)
12. L.H. Dubois, R.G. Nuzzo, Ann. Rev. Phys. Chem. **43**, 437 (1992)